# Supplementary Information

## Biocompatible and Label-Free Separation of Cancer Cells of Cell Culture Lines from White Blood Cells in Ferrofluids

Wujun Zhao,[a] Rui Cheng,[b] So Hyun Lim,[c] Joshua R. Miller,[a] Weizhong Zhang,[a] Wei Tang,[a] Jin Xie,[a] and Leidong Mao*[b]

[a]Department of Chemistry, University of Georgia, Athens, Georgia 30602, USA

[b]College of Engineering, University of Georgia, Athens, Georgia 30602, USA. E-mail: mao@uga.edu

[c]Department of Microbiology, University of Georgia, Athens, Georgia 30602, USA

**Three-dimensional model of cell transport in ferrofluids**

Cell trajectories are simulated in three-dimensional (3D) manner by modifying previously developed models with a concentration profile of ferrofluids across the width of the microchannel.[1, 2] We first calculate the 3D magnetic buoyancy force via an experimentally verified and analytical distribution of magnetic fields as well as their gradients, together with a nonlinear magnetization model of the ferrofluid. In order to simulate the magnetic field distribution in the channel generated from the permanent magnet, we followed the 3 steps as below:

1. We experimentally measured flux density at the center of magnet's polar surface, and points away from surface to obtain a flux density-distance relationship (see Fig. S1).
2. From the measured flux density-distance relationship, we determined the value of remnant magnetization of the permanent magnet. This value was used in the magnetic field simulation based on a set of governing equations,[1, 3] in order to generate a simulated flux density-distance relationship. We compared the experimental and simulated flux density-distance relationship and they were within 2.6% error range.
3. The simulated magnetic field distribution (flux density, strength, and gradient) was then confirmed to be valid and consistent with the measured values, and used in device optimizations.

The magnetic buoyancy force is expressed as,

$$\vec{F}_m = \mu_0 V_c \left[ \left( \vec{M}_c - \vec{M}_f \right) \cdot \nabla \right] \vec{H}$$

where $\mu_0 = 4\pi \times 10^{-7}$ H/m is the permeability of free space, $V_c$ is the volume of a single cell, $\vec{M}_c$ is its magnetization, $\vec{M}_f$ is magnetization of the magnetic fluid surrounding the body, and $\vec{H}$ is

the magnetic field strength at the center of the body. The magnetization of the ferrofluid $\vec{M}_f$ under an external field $\vec{H}$ is a Langevin function,

$$\vec{M}_f = \left( \coth(\alpha_f) - \frac{1}{\alpha_f} \right) \phi \vec{M}_{f,b}$$

where $\alpha_f = \mu_0 \pi M_{f,b} H d_f^3 \big/ 6 k_B T$. $M_{f,b}$ is saturation moments of the bulk magnetic materials, $d_f$ is diameters of magnetic nanoparticles in ferrofluid, $k_B$ is the Boltzmann constant and $T$ is the temperature. $\phi$ is the local concentration of the ferrofluid surrounding the cell, i.e., the concentration of the magnetic nanoparticles. Its expression is,

$$\phi(x,y) = \frac{\phi_0}{2} erfc\left( \frac{y - y_0}{\sqrt{D(x - x_0)/U}} \right)$$

where $\phi_0$ is the original volume fraction of magnetic nanoparticles in ferrofluid, ($x_0$, $y_0$) is the position of the mixing origin, $D$ is the diffusivity of magnetic nanoparticles and $U$ is the average velocity of the streams.

We then derived the hydrodynamic viscous drag force with an analytical velocity profile in the channel.

$$\vec{F}_d = -3\pi\eta D_p \left( \vec{U}_p - \vec{U}_f \right) f_D$$

where $\eta$ is viscosity of magnetic fluids, $D_p$ is diameter of a spherical particle, $\vec{U}_p$ and $\vec{U}_f$ are velocity vectors of the fluids and the particle respectively, $f_D$ is hydrodynamic drag force coefficient of a moving particle considering the influence with a solid surface in its vicinity, which is referred to as the "wall effect".[4-6]

We finally solved governing equations of motion using analytical expressions of magnetic buoyancy force and hydrodynamic viscous drag force. Because of the low Reynolds number in a microchannel, inertial effects on the particle are negligible. Motion of a non-magnetic particle in ferrofluids is determined by the balance of hydrodynamic viscous drag force and magnetic buoyancy force.

$$\vec{F}_m + \vec{F}_d = 0$$

This equation is solved by using a fourth-order Runge-Kutta time integration scheme in MATLAB.

**Magnetic convective mixing**

To evaluate the mixing performance within the devices, we used models developed from literatures on magnetic microfluidic mixing.[7-11] Similar to our experimental setup,[10] Nguyen's group used a non-uniform magnetic field to induce a body force on the ferrofluid stream and generate a convection of the ferrofluid into the water stream, achieving a rapid and efficient mixing. In our experiments, we also observed a fast mixing between the cell stream (inlet A) and the ferrofluid stream (inlet B) due to magnetic convection. All evidences indicated that the magnetic convection was much faster than diffusion, and was the dominant process in our devices.

To quantitatively estimate the minimal channel length $L_m$ needed for a homogeneous mixing between the cell stream and the ferrofluid stream, we first used the magnetic Peclet number $Pe_m$, which represented the ratio of the characteristic diffusion time over the characteristic time due to magnetic convection.[7]

$$Pe_m \equiv \frac{\mu_0 M^2 h^2}{\mu D}$$

where $\mu_0 = 4\pi \times 10^{-7}$ H/m is the permeability of free space, $M$, $h$, $\mu$ is the magnetization, the hydraulic diameter, and the viscosity of the ferrofluid, and $D$ is the diffusivity of the magnetic nanoparticles in the ferrofluid. According to Fig. S1 and Fig. S4a, $B$ = 125 mT in the microfluidic device and the magnetization of the ferrofluid $M$ = 639 A/m. The hydraulic diameter was estimated as the thickness of the channel $h$ = 52 $\mu$m, and viscosity of ferrofluids $\mu$ = 2.92 mPa·s. The diffusivity of the magnetic nanoparticles was obtained using the Stokes-Einstein relationship,

$$D \equiv \frac{\kappa_B T}{3\pi\mu d}$$

where $\kappa_B$ is Boltzmann's constant, $T$ is the temperature and $d$ is the diameter of the nanoparticles. From TEM analysis, $d$ = 11.24 nm. $D$ was estimated to be $1.34\times10^{-11}$ $m^2 \cdot s^{-1}$ in this case. Finally, the magnetic Peclet number $Pe_m$ in our case was $3.55\times10^4$, confirming that the magnetic convection was much faster than diffusion, and was the dominant process for mixing in our devices.

We then estimated the minimal channel length $L_m$ needed for a homogeneous mixing between the cell stream and the ferrofluid stream. For a complete mix between ferrofluid and buffer by diffusion alone, the characteristic diffusion length $l_d$ should be less than the total width of the channel, i.e., $l_d \leq 900$ $\mu$m in our devices. The associated characteristic diffusion time $t_d$ was calculated via,

$$t_d \equiv \frac{l_d^2}{D}$$

Here, we obtained $t_d = 6\times10^4$ s. Based on the definition of $Pe_m$, the characteristic time of magnetic convection $t_c$ = 1.7 s. Considering the average velocity of the flow $U_f$ = 3.1~16.2mm/s,

i.e., flow rate 8.5~45 μL/min, in our devices, the minimal channel length $L_m$ needed for a homogeneous mixing between the cell stream and the ferrofluid stream was estimated to be 1.6-8.3 mm.

**Verification of device optimization using cancer cell lines and red blood cells**

In order to verify the device and fluid optimization, we used two cancer cell lines and diluted whole blood (mainly red blood cells) for verification. We used the following parameters: cell flow rate (15 $\mu$L/min, i.e., 0.9 mL/h), magnetic field and gradient (134 mT, 32.2 T/m), and ferrofluid concentration (0.26% v/v) based on optimization and calibration results. Mean diameters of all cells used here were measured to be: 15.5 $\mu$m for A549, 18.7 $\mu$m for MCF-7, 6.5 $\mu$m for RBCs.

We used two types of cancer cells (A549 lung cancer and MCF-7 breast cancer) with a spike ratios of 100 cells/mL. Human whole blood was diluted with PBS to have a concentration of $10^6$ cells/mL for such experiments. Experimental results are summarized in Fig. S5 and Table S1. Fig. S5a shows a composite image when magnetic fields were not present, A549 cancer cells and RBCs were flowing near the bottom of the channel and exiting through the outlet 1, resulting in no separation of the two. Fig. S5b shows a composite image when magnetic fields were present, magnetic buoyancy forces deflected larger A549 cancer cells from the ferrofluid stream into the PBS buffer stream toward outlet 4. Meanwhile, magnetic forces on smaller RBCs were insufficient to deflect them to the buffer stream. Therefore, RBCs remained in the ferrofluid stream and exited through outlets 2 and 3. This was confirmed by a fluorescence image in Fig. S5c, where A549 cells labeled with green fluorescence were observed to exit mainly from outlet 4. Table S1 summarizes the separation performance. The separation efficiency (defined as the

ratio of captured cancer cells to spiked cancer cells) for A549 cells was 77±6%. The purity of cancer cells (defined as the ratio of cancer cells to all cell types in outlet 4) was 62.1±0.9%. Similar experiments were carried out to separate MCF-7 breast cancer cells from diluted whole blood. Its separation efficiency was 84±4%, and purity of cancer cells was 59.2±0.8%. This size-based separation strategy performed well in separating cancer cells from diluted whole blood, because of significant size differences between cancer cells and RBCs. As the diameter of cancer cells increased from 15.5 $\mu$m (A549) to 18.7 $\mu$m (MCF-7), we observed slight increase in separation efficiency.

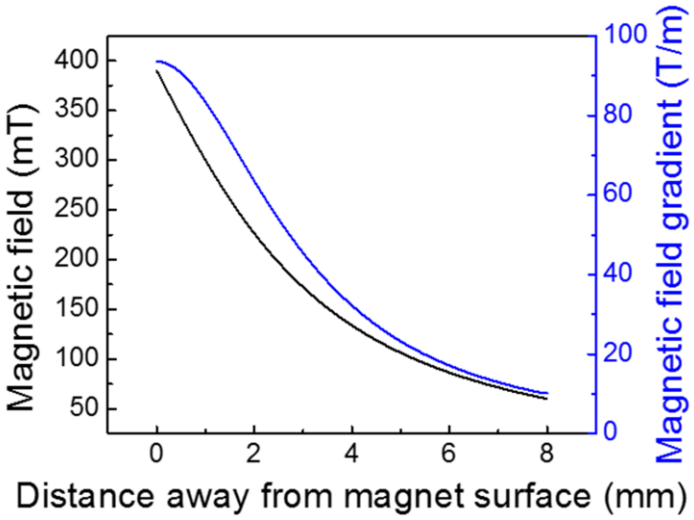


**Fig. S1.** Measured magnetic field and its gradient of the center of magnet's surface vs. distance away from the surface.

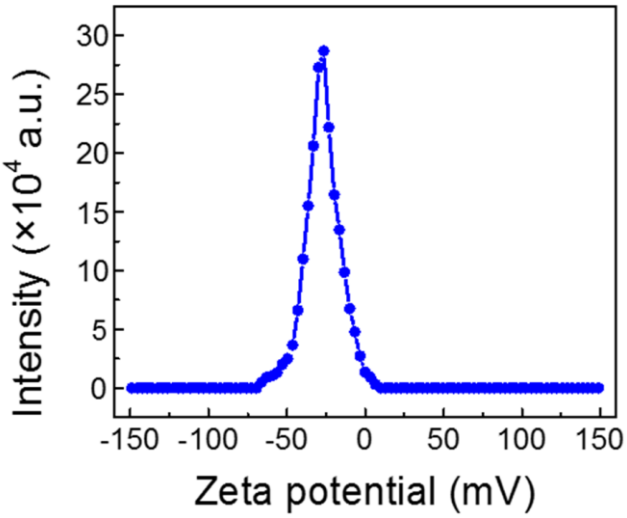


**Fig. S2.** Zeta potential of the ferrofluid was measured to be -27.2±11.4 mV.

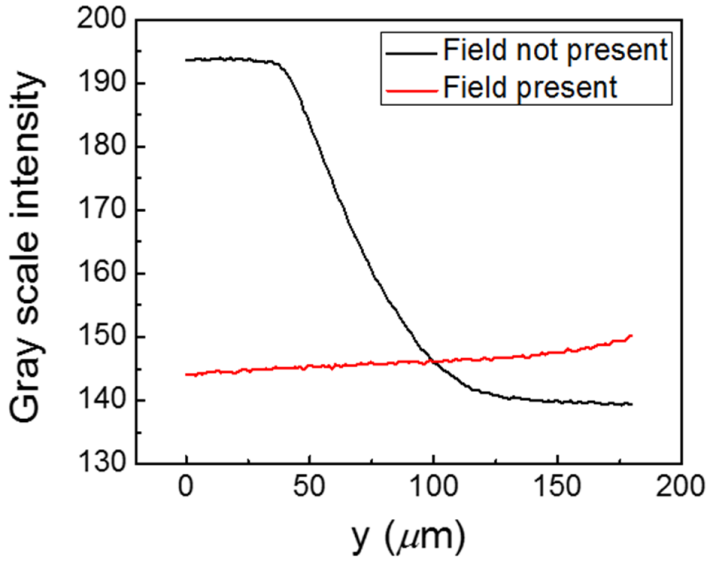


**Fig. S3.** The mean gray scale intensity in the red boxes of Fig. 4(d) and (e) (main text) as a function of channel width.

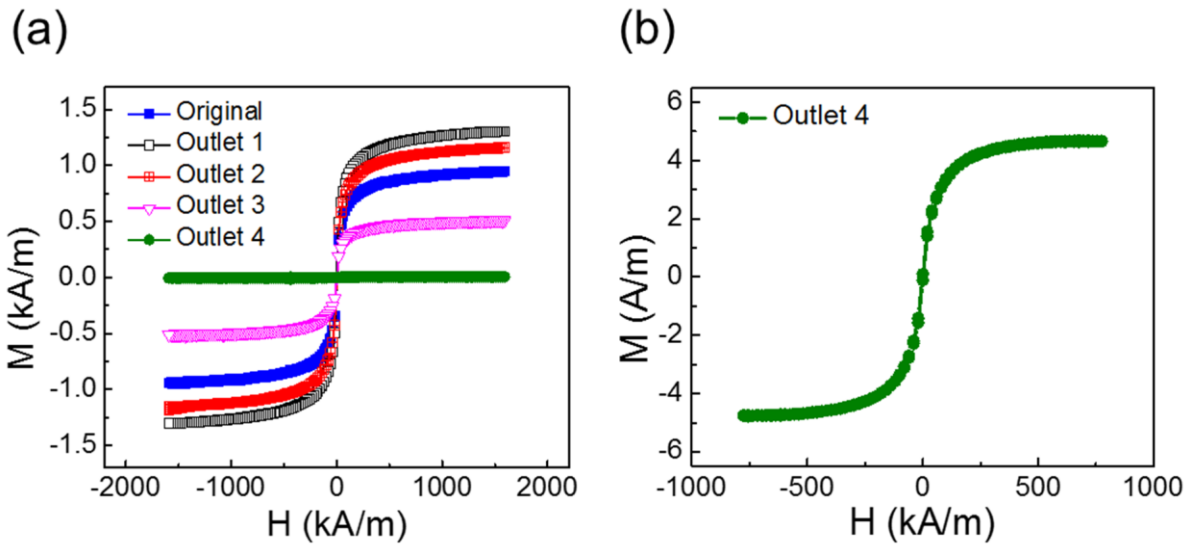


**Fig. S4.** (a) Magnetizations of the original ferrofluid (blue) and ferrofluids collected from each outlet. Ferrofluids collected from outlets 1 and 2 (black and red) had higher concentrations of magnetic nanoparticles, possibly due to the attraction of the permanent magnet. Ferrofluids collected from outlet 3 (purple) had approximately half concentration of the nanoparticles in the original ferrofluid. Ferrofluids collected from outlet 4 had significantly less nanoparticles than the original ferrofluid. (b) Magnetization of ferrofluids collected from outlet 4. Saturation magnetization was measured to be 4.75 A/m, corresponding to a 0.00128% volume fraction of magnetic materials. For comparison, the original ferrofluid had a 0.26% volume fraction of magnetic materials.

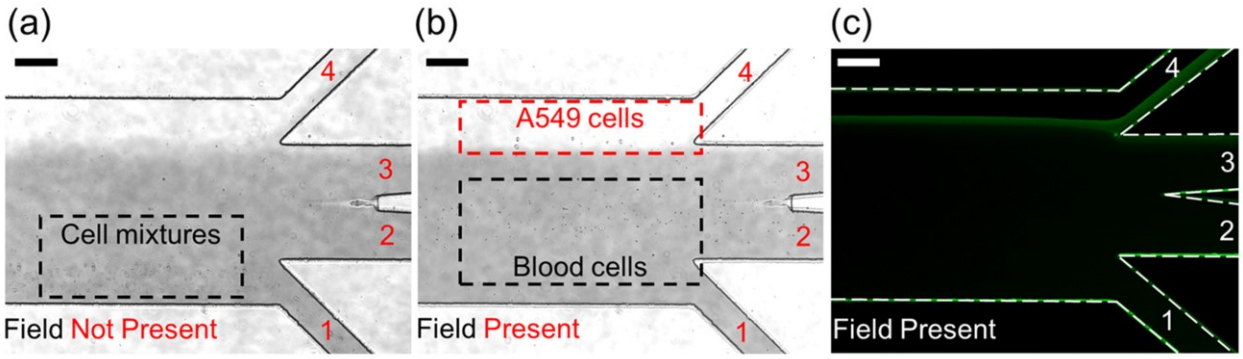


**Fig. S5.** Micrographs of cancer cell separation processes. (a) In absence of magnetic fields, cell mixtures exited the channel through outlet 1. (b) When magnetic fields were present, larger A549 cancer cells were deflected and reached the ferrofluid/buffer boundary, exited through outlet 4 (collection outlet), while smaller blood cells exited through other outlets. (c) Fluorescence images of A549 cancer cells during cell separation. A549 cells were stained by CellTracker Green. Dashed white lines depict the microchannel boundaries. Scale bars: 200 $\mu$m.

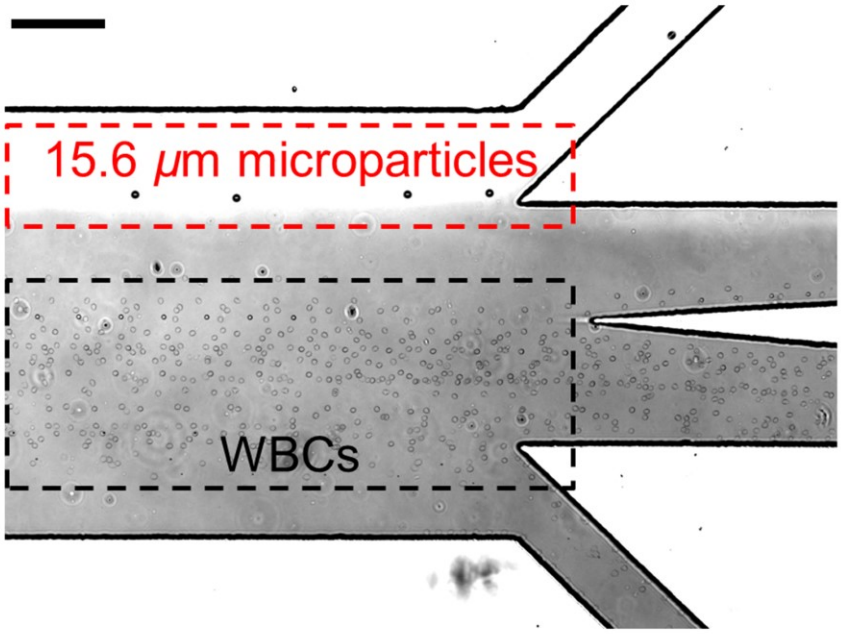


**Fig. S6.** Calibration of 15.6 $\mu$m microparticles and white blood cells (WBCs). Scale bar: 200 $\mu$m.

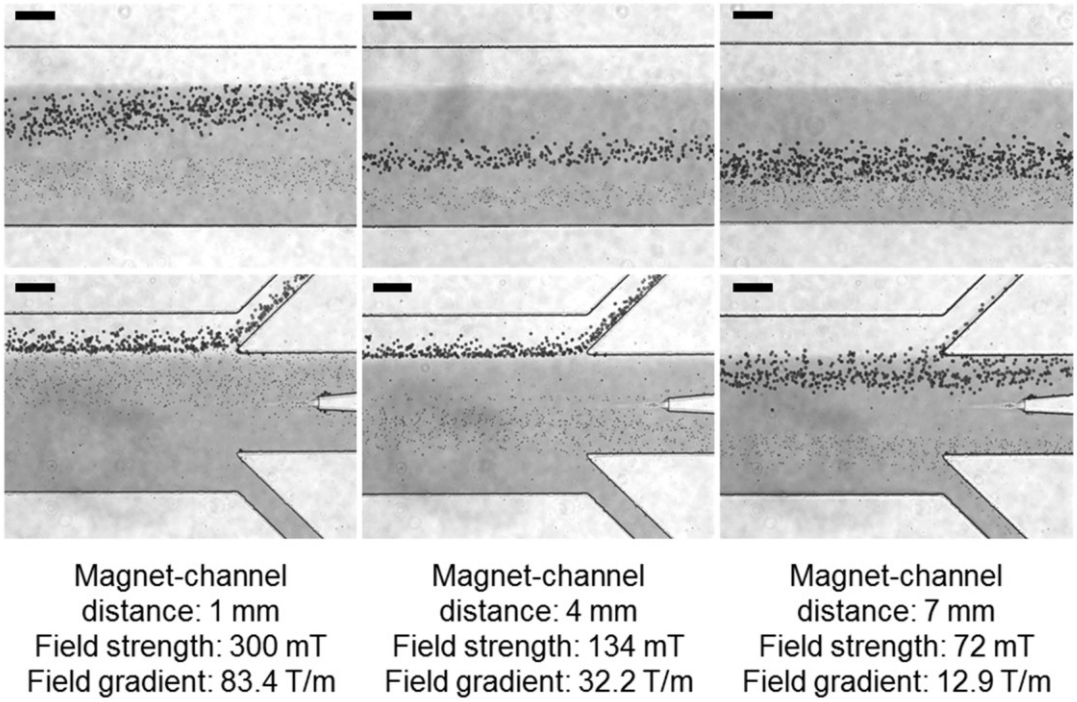


**Fig. S7.** Representative images of microparticle separation when the magnet-channel distance was 1 mm, 4 mm, and 7 mm, respectively. Two types of microparticles (15.7 $\mu$m and 5.8 $\mu$m) were used in the calibration. Flow rates of inlet A and inlet B were fixed at 4 and 5 $\mu$L/min, respectively. Flow rate of inlet C was changed accordingly to adjust the buffer/ferrofluid boundary just right below the outlet 4. Ferrofluid with concentration of 0.26% (v/v) was used. Scale bars: 200 $\mu$m.

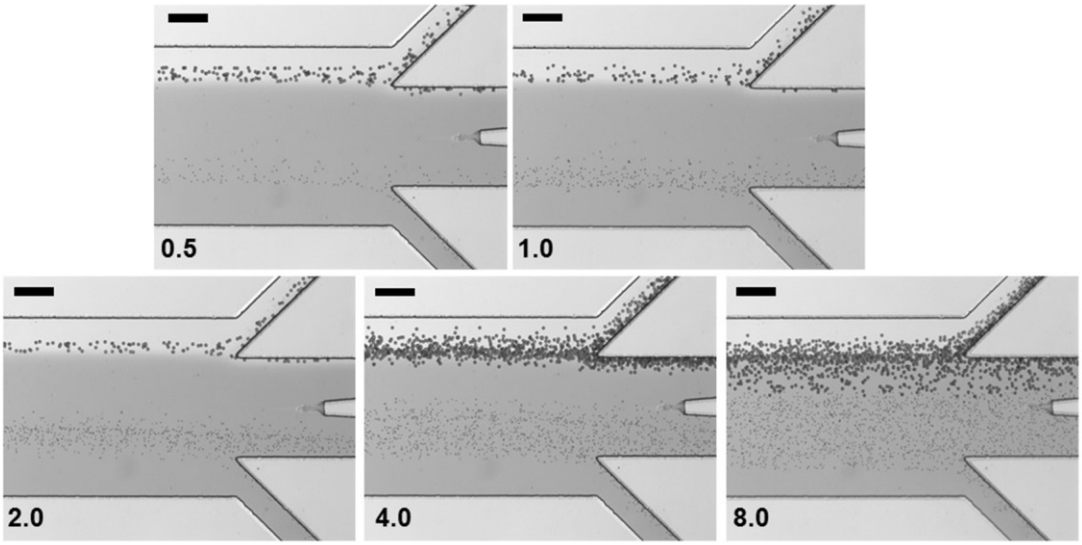


**Fig. S8.** Representative images of microparticle separation at different flow rates of cell inlet A. Numbers in each figure indicate the flow rates (unit: $\mu$L/min) of inlet A. Magnet was placed 4 mm away from the channel and 0.26% (v/v) ferrofluid was used. Flow rate of inlet B was fixed at 5 $\mu$L/min. Flow rate of inlet C was changed accordingly to adjust the buffer/ferrofluid boundary just right below the outlet 4. Scale bars: 200 $\mu$m.

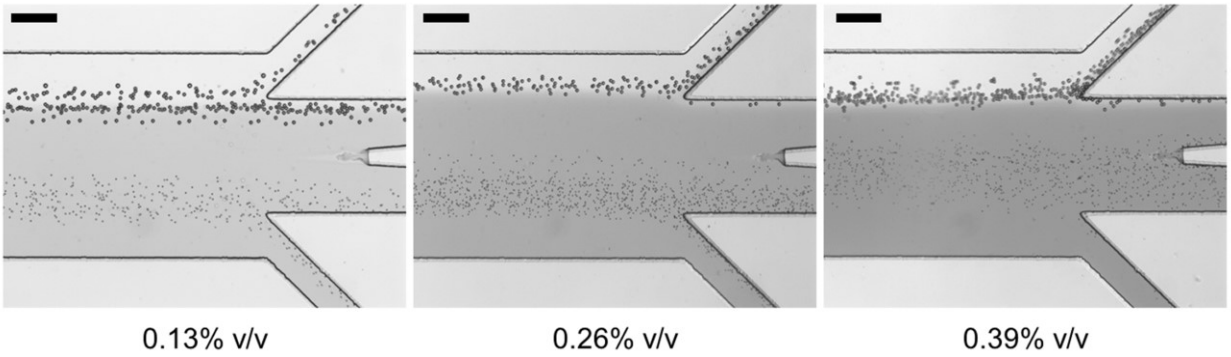


**Fig. S9.** Representative images of microparticle separation at different concentrations of ferrofluids (0.13, 0.26, and 0.39% v/v). Magnet was placed 4 mm away from the channel. Flow rate of inlet A and inlet B were fixed at 4 and 5 $\mu$L/min, respectively. Flow rate of inlet C was changed accordingly to adjust the buffer/ferrofluid boundary just right below the outlet 4. Scale bars: 200 $\mu$m.

**Table S1.** Summary of cancer cell separation performance

| Cell line | No. of cells spiked | No. of cells captured | Efficiency | No. of WBCs | Purity |
|---|---|---|---|---|---|
| A549 | 100 | 77±6 | 77±6% | 47±11 | 62.1±0.9% |
| MCF-7 | 100 | 84±4 | 84±4% | 58±18 | 59.2±0.8% |

100 CellTracker Green stained cancer cells were spiked into 1 mL of diluted whole blood (1000-time dilution, mostly RBCs). Data are expressed as Mean±S.D., n=3.

## References


1. R. Cheng, T. T. Zhu and L. D. Mao, *Microfluid Nanofluid*, 2014, **16**, 1143-1154.
2. T. T. Zhu, D. J. Lichlyter, M. A. Haidekker and L. D. Mao, *Microfluid Nanofluid*, 2011, **10**, 1233-1245.
3. E. P. Furlani, *Permanent magnet and electromechanical devices : materials, analysis, and applications*, Academic, San Diego, Calif. ; London, 2001.
4. P. Ganatos, S. Weinbaum and R. Pfeffer, *Journal of Fluid Mechanics*, 1980, **99**, 739-753.
5. G. P. Krishnan and J. David T. Leighton, *Physics of Fluids*, 1995, **7**, 2538-2545.
6. M. E. Staben, A. Z. Zinchenko and R. H. Davis, *Physics of Fluids*, 2003, **15**, 1711-1733.
7. C. Y. Wen, K. P. Liang, H. Chen and L. M. Fu, *Electrophoresis*, 2011, **32**, 3268-3276.
8. G. P. Zhu and N. T. Nguyen, *Lab Chip*, 2012, **12**, 4772-4780.
9. G. P. Zhu, M. Hejiazan, X. Y. Huang and N. T. Nguyen, *Lab Chip*, 2014, **14**, 4609-4615.
10. M. Hejazian and N. T. Nguyen, *Micromachines-Basel*, 2017, **8**.
11. L. Mao and H. Koser, OVERCOMING THE DIFFUSION BARRIER: ULTRA-FAST MICRO-SCALE MIXING VIA FERROFLUIDS. The 14th International Conference on Solid-State Sensors, Actuators and Microsystems; 2007 June 10-14, 2007; Lyon, France